Mon. Not. R. Astron. Soc. **330,** 129–136 (2002)

Smoothed Particle Hydrodynamics with particle splitting, applied to self-gravitating collapse

S. Kitsionas★† and A. P. Whitworth★

Department of Physics & Astronomy, Cardiff University, PO Box 913, 5 The Parade, Cardiff CF24 3YB

Accepted 2001 October 12. Received 2001 August 23; in original form 2000 July 5

ABSTRACT

We describe and demonstrate a method for increasing the resolution locally in a Smoothed Particle Hydrodynamic (SPH) simulation, by splitting particles. We show that in simulations of self-gravitating collapse (of the sort that are presumed to occur in star formation) the method is stable, and affords great savings in computer time and memory. When applied to the standard Boss & Bodenheimer test – which has been shown to depend critically on fulfilment of the Jeans Condition – the results are comparable both with those obtained using Adaptive Mesh Refinement, and with those obtained using a standard high-resolution SPH simulation, but they are achieved with considerably less computational resource. Further development and testing is required before the method can safely be applied to more general flows.

Key words: gravitation – hydrodynamics – methods: numerical – stars: formation.

1 INTRODUCTION

Numerical simulations of star formation – even the highly idealized simulations to which contemporary astrophysics is limited – require very large computational resources. The dynamics is self-gravitating, so the gravitational field has to be recalculated at each time-step. The ranges of density ($\sim 10^{-22}\,\mathrm{g\,cm^{-3}}$ to $\sim 10^{1}\,\mathrm{g\,cm^{-3}}$) and linear scale ($\sim 10^{20}\,\mathrm{cm}$ to $\sim 10^{10}\,\mathrm{cm}$) are very large, so high resolution is needed. The geometry is complex, so three-dimensional simulations are essential. The dynamics is affected by a variety of radiative, thermal, chemical and magnetic effects, with the result that the energy equation is not a local function of state. The initial and boundary conditions are chaotic and poorly constrained by observation.

Smoothed Particle Hydrodynamics (SPH) is a particle-based hydrodynamic scheme which accommodates some of these requirements automatically, by virtue of being Lagrangian, having no imposed geometrical constraints, and being readily combined with particle-based gravity solvers, for example Tree Code Gravity (TCG; Barnes & Hut 1986; Hernquist 1987; Hernquist & Katz 1989). SPH is also relatively straightforward to implement, at least in its most basic formulation. More refined versions have to be used to obtain realistic results when there are large gradients of density (e.g. shocks and ionization fronts) and/or velocity (e.g. shocks and rapidly shearing discs).

Since its initial realization (Lucy 1977; Gingold & Monaghan 1977), SPH has been developed and refined by several workers, for example Lattanzio et al. (1985; artificial viscosity), Nelson & Papaloizou (1993, 1994; variable h), Bate, Bonnell & Price (1995; sink particles), Watkins et al. (1995; Navier–Stokes viscosity), Morris & Monaghan (1997; time-varying artificial viscosity), Nelson & Langer (1997; scheme for treating the thermal physics), Owen et al. (1998; tensorial smoothing kernels), Inutsuka & Imaeda (2001; Godunov scheme for interparticle hydro forces) and Kessel-Deynet & Burkert (2000; scheme for following ionization fronts).

The principle alternatives to SPH are finite difference (FD) codes, or hybrids that combine particles and cells. FD codes are much better at resolving large density and/or velocity gradients. They should probably be the method of choice for simulating flows with high Mach Number. However, in three dimensions they are not as easy to implement as SPH, and they are not Lagrangian. Moreover, it should be born in mind that FD codes benefit from having had very many more person-years of development than SPH.

In FD codes, the high local resolution required for calculations of protostellar collapse can be obtained by means of nested grids. These nested grids can either be introduced at the outset to cover places where it is anticipated that extra resolution will be required (e.g. Burkert & Bodenheimer 1993); or they can be introduced and removed during the course of the simulation, whenever and wherever they are required, as in Adaptive Mesh Refinement (AMR: Berger & Colella 1989; Truelove et al. 1997, 1998). With AMR, the resolution can, in principle, be increased indefinitely in regions where this is necessary.

In standard SPH, the linear resolution is $\sim(m/\rho)^{1/3}$, where m is the mass of an individual particle and ρ is the local density. In this paper we describe a rather straightforward algorithm whereby the resolution of an SPH code can also, in principle, be increased

★E-mail: spyrmyr@hotmail.com (SK); ant@astro.cf.ac.uk (AW)
†Present address: 14 John Kennedy str., 16121 Kesariani, Athens, Greece.

indefinitely, by splitting particles. We test the method on the standard Boss & Bodenheimer (1979) test, using the Jeans condition to trigger splitting. Particle splitting and merging were used by Meglicki, Wickramasinghe & Bicknell (1993) in their simulations of accretion discs, and particle merging had been used earlier by Monaghan & Varnas (1988) in simulations of interstellar cloud complexes. However, in these earlier implementations splitting was used to maintain resolution in low-density regions, and merging was used to avoid following large numbers of particles in high-density regions (essentially the motivation for sink particles; Bate et al. 1995). Therefore, the philosophy was very different from that adopted here, where high resolution is advocated in high-density regions to avoid violating the Jeans condition (i.e. to ensure resolution of the local Jeans mass). Moreover, no tests were reported in these earlier papers.

Section 2 gives a brief review of standard SPH. Section 3 sketches the implementation of Particle Splitting, at the microscopic level, and Section 4 describes how the best parameters for Particle Splitting are determined. Sections 5 and 6 describe two algorithms for Particle Splitting at the macroscopic level. In Nested Splitting (Section 5) all the particles in a prescribed subdomain are split from some predetermined time $t_{\rm split}$ onwards, so that in effect a high-resolution simulation is performed inside the subdomain using initial and boundary conditions supplied by the coarser simulation in the overall computational domain. In On-The-Fly Splitting (Section 6), particles are split only when this is necessary according to some local criterion such as the Jeans Condition. On-The-Fly Splitting is the more computationally efficient procedure, requiring no manual intervention and no prior knowledge of where high resolution will be required; it corresponds closely to AMR. Section 7 introduces the Jeans Condition, and Section 8 demonstrates how effectively and economically SPH performs the standard Boss & Bodenheimer (1979) rotating collapse test when Particle Splitting is included. Section 9 discusses the results and compares them with those obtained using AMR. Our conclusions are summarized in Section 10.

2 BASIC SMOOTHED PARTICLE HYDRODYNAMICS AND TREE-CODE GRAVITY

In SPH the evolution of the gas is predicted by following the motions of an ensemble of $i_{\rm total}$ particles which act as discrete sampling points (e.g. Monaghan 1992). Each particle has associated with it a mass m_i, smoothing length h_i, position $\boldsymbol{r}_i$, velocity $\boldsymbol{v}_i$, and values for any other local intensive thermodynamic variables required to describe the state of the gas, for example density ρ_i, pressure P_i, specific internal energy u_i, magnetic field $\boldsymbol{B}_i$, etc.

At an arbitrary position $\boldsymbol{r}$, the value of any physical variable A can be obtained by interpolating over the values of A associated with nearby particles, using a smoothing kernel W, namely

$$A(\boldsymbol{r}) = \sum_i \left\{ \frac{A_i m_i}{\rho_i h_i^3} W\left(\frac{|\boldsymbol{r} - \boldsymbol{r}_i|}{h_i} \right) \right\}. \tag{1}$$

The kernel is normalized,

$$\int_{s=0}^{s=\infty} W(s) 4\pi s^2 \, {\rm d}s = 1, \tag{2}$$

and has compact support [specifically $W(s > 2) = 0$], so that the sum is over a finite number $\mathcal{N}_{\rm neib}$ of neighbouring particles.

The gradient of A can then be evaluated from

$$\nabla A(\boldsymbol{r}) = \sum_i \left\{ \frac{A_i m_i}{\rho_i h_i^4} W'\left(\frac{|\boldsymbol{r} - \boldsymbol{r}_i|}{h_i} \right) \frac{\boldsymbol{r} - \boldsymbol{r}_i}{|\boldsymbol{r} - \boldsymbol{r}_i|} \right\}, \tag{3}$$

where $W'(s) \equiv {\rm d}W/{\rm d}s$.

The motions of the particles are driven by interparticle forces representing the local pressure gradient, viscosity, gravity and magnetic field. Interparticle forces are formulated symmetrically so that linear and angular momentum are conserved. In our basic implementation we use the M4 kernel introduced by Monaghan & Lattanzio (1985). The particles all have the same mass. We omit magnetic fields.

The smoothing length h_i is varied so that the kernel contains $\mathcal{N}_{\rm neib} \sim 50(\pm 5)$ particles. This ensures that the spatial resolution becomes finer with increasing density.

The density at the position of particle i is given by

$$\rho_i = \sum_j \left\{ \frac{m_i}{\bar{h}_{ij}^3} W\left(\frac{|\Delta \boldsymbol{r}_{ij}|}{\bar{h}_{ij}} \right) \right\}, \tag{4}$$

where

$$\bar{h}_{ij} = \frac{h_i + h_j}{2}, \qquad \Delta \boldsymbol{r}_{ij} = \boldsymbol{r}_i - \boldsymbol{r}_j,$$

The sum in equation (4) is over the $\sim \mathcal{N}_{\rm neib}$ neighbours within $2\bar{h}_{ij}$, and it includes particle i itself.

In many applications, the pressure at particle i is given by a barotropic equation of state $P_i = P(\rho_i)$. In this case there is no need to solve an energy equation.

The gravitational acceleration of a particle can be obtained by a direct sum of the contributions from all the other particles,

$$\boldsymbol{g}_i = -\sum_{j \neq i} \left\{ \frac{G m_j}{|\Delta \boldsymbol{r}_{ij}|^2} \frac{\Delta \boldsymbol{r}_{ij}}{|\Delta \boldsymbol{r}_{ij}|} \right\}. \tag{5}$$

However, there are two problems with this approach. The first problem arises because individual particles are very massive. As a result, close interactions between particles (small $|\Delta \boldsymbol{r}_{ij}|$) lead to artificially large accelerations which corrupt the simulation. This can be cured by softening the mutual gravity of any two particles having small separation. The form of softening we use assumes that the kernel describes the distribution of a particle's mass, and then invokes Gauss's Gravitational Theorem. The effect is to introduce a term $W^*(|\Delta \boldsymbol{r}_{ij}|/h_{\tilde{ij}})$ into the sum of equation (5) (see equation 8, below), where

$$W^*(s) = \int_{s'=0}^{s'=s} W(s') 4\pi s'^2 \, {\rm d}s'. \tag{6}$$

The second problem arises because the cost of computing the sum in equation (5) for all the particles increases as $i_{\rm total}^2$ (where $i_{\rm total}$ is the total number of particles). Since the linear resolution, and the time-step, of an SPH simulation are proportional to $i_{\rm total}^{-1/3}$, the cost of increasing the resolution soon becomes prohibitive. An effective solution to this problem is to arrange the particles in an hierarchical octal tree structure, i.e. a nested grid of cells within cells. This is called Tree-Code Gravity (TCG: Barnes & Hut 1986; Hernquist 1987).

The top cell of the tree is the entire computational domain, assumed here to be a cube. The top cell is then partitioned into eight equal cubic sub-cells, these in turn are each divided into eight equal cubic sub-sub-cells, and so on. Partitioning is continued until

the lowest cells in the tree contain either one particle or no particle. Then the mass M_I, centre of mass $\boldsymbol{R}_I$, linear size L_I and quadrupole moment $\boldsymbol{Q}_I$ of each cell I are calculated and stored (along with some other cell parameters which are useful for finding neighbours).

When the gravitational acceleration of particle i is being computed, the contribution from a distant cell can be evaluated to sufficient accuracy using its M_I, $\boldsymbol{R}_I$, $\boldsymbol{Q}_I$, and there is no need to consider its constituent particles individually. For particle i at $\boldsymbol{r}_i$, cell I at position $\boldsymbol{R}_I$ is sufficiently distant to justify this approximation if

$$L_I < \theta_{\rm crit}|\boldsymbol{R}_I - \boldsymbol{r}_i|, \tag{7}$$

with $\theta_{\rm crit} = 0.576$ (Salmon, Warren & Winckelmans 1994).

The equation of motion for particle i is then

$$\frac{d\boldsymbol{v}_i}{dt} = -\sum_j \left\{ \frac{m_i}{\bar{h}_{ij}^4}\left[\frac{P_i}{\rho_i^2} + \frac{P_j}{\rho_j^2} + \Pi_{ij}\right] W'\left(\frac{|\Delta\boldsymbol{r}_{ij}|}{\bar{h}_{ij}}\right)\frac{\Delta\boldsymbol{r}_{ij}}{|\Delta\boldsymbol{r}_{ij}|}\right\}$$
$$- \sum_{j\neq i}\left\{\frac{m_j}{|\Delta\boldsymbol{r}_{ij}|^2} W^*\left(\frac{|\Delta\boldsymbol{r}_{ij}|}{\bar{h}_{ij}}\right)\frac{\Delta\boldsymbol{r}_{ij}}{|\Delta\boldsymbol{r}_{ij}|}\right\}. \tag{8}$$

Here, the first sum represents short-range forces (hydrostatic and viscous forces) and is only over nearby particles. The second sum gives the gravitational acceleration, which is long-range, and is nominally over all particles. In practice, distant particles are grouped into clusters using the TCG algorithm, as described in the preceding paragraphs.

Π_{ij} is the artificial viscosity term advocated by Lattanzio et al. (1985), namely

$$\Pi_{ij} = \begin{cases} \dfrac{-\alpha\mu_{ij}\bar{c}_{ij} + \beta\mu_{ij}^2}{\bar{\rho}_{ij}}, & \mu_{ij} < 0; \\ 0, & \mu_{ij} > 0; \end{cases} \tag{9}$$

where

$$\mu_{ij} = \frac{(\Delta\boldsymbol{v}_{ij}\cdot\Delta\boldsymbol{r}_{ij})\bar{h}_{ij}}{|\Delta\boldsymbol{r}_{ij}|^2 + 0.01\bar{h}_{ij}^2}, \tag{10}$$

$\Delta\boldsymbol{v}_{ij} \equiv \boldsymbol{v}_i - \boldsymbol{v}_j$, $\bar{c}_{ij} = (c_i + c_j)/2$ and $\bar{\rho}_{ij} = (\rho_i + \rho_j)/2$. We have used $\alpha = 1$ and $\beta = 1$.

The equation of motion is integrated using a second-order Runge–Kutta scheme:

$$\boldsymbol{a}_i^n = \boldsymbol{a}(\boldsymbol{r}_i^n, \boldsymbol{v}_i^n);$$

$$\boldsymbol{r}_i^{n+\frac{1}{2}} = \boldsymbol{r}_i^n + \boldsymbol{v}_i^n\frac{\Delta t}{2};$$

$$\boldsymbol{v}_i^{n+\frac{1}{2}} = \boldsymbol{v}_i^n + \boldsymbol{a}_i^n\frac{\Delta t}{2};$$

$$\boldsymbol{a}_i^{n+\frac{1}{2}} = \boldsymbol{a}\left(\boldsymbol{r}_i^{n+\frac{1}{2}}, \boldsymbol{v}_i^{n+\frac{1}{2}}\right);$$

$$\boldsymbol{r}_i^{n+1} = \boldsymbol{r}_i^n + \boldsymbol{v}_i^{n+\frac{1}{2}}\Delta t;$$

$$\boldsymbol{v}_i^{n+1} = \boldsymbol{v}_i^n + \boldsymbol{a}_i^{n+\frac{1}{2}}\Delta t;$$

where $\boldsymbol{r}_i^n, \boldsymbol{v}_i^n$ and $\boldsymbol{a}_i^n$ are the position, velocity and acceleration of particle i at time-step n.

The code invokes a binary hierarchy of multiple particle time-steps, $\Delta t_k^* = 2^{-k}\Delta t_{\rm max}^*$ with $k = 0, 1, 2, \ldots, k_{\rm max} = 30$. For each particle i we evaluate a maximum time-step according to

$$\Delta t_i = 0.3\,{\rm MIN}\left\{\frac{1}{|\nabla\cdot\boldsymbol{v}|_i}, \frac{h_i}{|\boldsymbol{v}|_i}, \left(\frac{h_i}{|\boldsymbol{a}|_i}\right)^{1/2}, \frac{h_i}{\sigma_i}\right\} \tag{11}$$

where

$$\sigma_i = c_i + 1.2(\alpha c_i + \beta\,{\rm MAX}\{\mu_{ij}\}). \tag{12}$$

The particle is then given the largest time-step Δt_k^* from the binary hierarchy that is smaller than Δt_i, i.e.

$$k = \log_2\left\{\frac{\Delta t_{\rm max}^*}{\Delta t_i}\right\} + 1, \qquad \Delta t_i \rightarrow \Delta t_k^*. \tag{13}$$

A more detailed description of the basic code can be found in Turner et al. (1995).

3 PARTICLE SPLITTING

The resolution of SPH is of order the local smoothing length h, and with $\mathcal{N}_{\rm neib} \sim 50$, $h \sim (m/\rho)^{1/3}$. Therefore in order to improve the resolution of a simulation locally we need to reduce the masses of the individual particles, and hence to increase the overall number of particles.

In Particle Splitting, this is done by replacing individual particles (parent particles) with small groups of particles (families of children particles). In the standard form of SPH, an individual particle is spherically symmetric, by virtue of having an isotropic smoothing kernel. Therefore we should distribute the family of child particles that replace it so that the sum of their smoothing kernels is approximately spherically symmetric.

This is achieved by creating 13 children, each with mass

$$m_{\rm child} = \frac{m_{\rm parent}}{13}. \tag{14}$$

The children are then placed on an hexagonal close-packed array, with the first child at the same position as the parent, and the other twelve children equidistant from the first; the method used to determine the optimum value for the distance ℓ between the first child and each of its siblings is described in the next section. Finally the array of particles is rotated to an arbitrary orientation.

The choice of 13 children is a compromise between two considerations. On the one hand, there should not be too large a disparity between parent mass and child mass, otherwise there will be greatly increased numerical diffusion wherever parents and children are neighbours. On the other hand, it is desirable that the collective density distribution of the family of children approximate to the spherically symmetric density distribution of their parent. With 13 children there is a relatively small variance in the collective density of the children on a spherical surface centred on the position of the parent.

4 FINE-TUNING THE FAMILY OF CHILD PARTICLES

The child particles are initially given smoothing lengths

$$h_{\rm child} = (13)^{-1/3}h_{\rm parent}, \tag{15}$$

so that they have the same net volume as their parent particle.

Two experiments have been preformed to determine the optimum value for ℓ (the distance between the first child and each of its twelve siblings).

In the first experiment we take a microscopic approach. We consider a single parent particle and compute the volume-weighted

difference between its density and the combined densities of its children:

$$\int_{\text{all space}} \left| \sum_{i'} \{\rho_{i'}(\boldsymbol{r})\} - \rho_{\text{parent}}(\boldsymbol{r}) \right| \mathrm{d}^3\boldsymbol{r}, \tag{16}$$

where the summation index i' represents the identifiers of the children. This quantity has its minimum value when $\ell \simeq 1.9h_{\text{child}}$, but it is still quite large, $\sim 0.33m_{\text{parent}}$.

In the second experiment we take a macroscopic approach. 500 equal-mass particles are distributed randomly inside a cube. They are then settled using SPH with uniform sound speed and periodic boundary conditions, until the density is very uniform, specifically $\sigma_\rho/\bar{\rho} < 0.01$. Then we split all the particles simultaneously and resettle them. For $\ell = 1.5h_{\text{child}}$, the value of $\sigma_\rho/\bar{\rho}$ is a minimum (~ 0.10) immediately after splitting, and the time required to settle back to $\sigma_\rho/\bar{\rho} < 0.01$ is also a minimum. The minimum of $\sigma_\rho/\bar{\rho}$ immediately after splitting is quite shallow (it increases to ~ 0.12 for $\ell \simeq 1.2h_{\text{child}}$, and for $\ell \simeq 2.0h_{\text{child}}$), and this is largely testimony to the smoothing ability of the M4 kernel used with ~ 50 neighbours (Monaghan & Lattanzio 1985).

We believe that this second experiment is the more relevant, as it is the macroscopic properties of the fluid that SPH seeks to mimic. In other words, it is the continuous density and velocity fields (which at most positions are compounded by contributions from $\sim \mathcal{N}_{\text{neib}}$ particles) that SPH must aspire to reproduce, and not the density of a single parent particle.

All subsequent tests are therefore performed with $\ell = 1.5h_{\text{child}}$.

5 NESTED SPLITTING

One way to implement Particle Splitting is to start a standard simulation at $t = 0$, then at $t = t_{\text{split}} (\geq 0)$ to identify a part of the overall computational domain, i.e. a subdomain, where improved resolution is required or desired, and to split all particles in this subdomain. In the sequel we refer to the initial standard simulation and the particles in it as – respectively – the coarse simulation and the coarse particles. We refer to the simulation after t_{split} and the split particles in the subdomain as – respectively – the fine simulation and the fine particles.

At time $t = t_{\text{split}}$ the newly created fine child particle i' is given a velocity by summing contributions from the ~ 50 neighbours (index j) of – and including – the coarse parent particle (index i):

$$\boldsymbol{v}_{i'} = \sum_j \left\{ \frac{m_j \boldsymbol{v}_j}{\rho_j \bar{h}_{ij}^3} W\left(\frac{|\boldsymbol{r}_{i'} - \boldsymbol{r}_j|}{\bar{h}_{ij}} \right) \right\}. \tag{17}$$

Thereafter ($t > t_{\text{split}}$), any coarse parent particle that enters the subdomain is immediately split and the resulting fine child particles are again given velocities by summing over the neighbours of the coarse parent particle. The densities and accelerations of fine particles are calculated using the standard SPH equations (equations 4 and 8).

Near the boundary of the subdomain, there are coarse particles that have fine particles as neighbours, and vice versa. Because of this, we have to revise the way in which the smoothing lengths of particles are adjusted. The results are greatly improved if, instead of requiring the number of neighbours of particle i to be ~ 50, we require the total mass of the neighbours of particle i to be ~ 50 times the mass of particle i, i.e.

$$\sum_j \{m_j\} \sim 50 m_i. \tag{18}$$

For fine particles well inside the subdomain, and for coarse particles well outside the subdomain, this makes no difference, but it is important for particles near the boundary, including coarse particles that are about to be split.

6 ON-THE-FLY SPLITTING

A second way to implement Particle Splitting is to identify particles with resolution, $\sim (m/\rho)^{1/3}$, that is insufficient for the problem in hand, and split them on-the-fly. To do this, we must recognize what the deterministic physics of the problem is, and quantify – as a local function of state – the minimum resolution required to capture this physics. Then, whenever the resolution of a particle approaches the local minimum resolution, that particle is split.

As in Nested Splitting, the velocities of the new child particles are evaluated by summing contributions from the neighbours of the parent particle. Successive generations of splitting are possible, yielding particles with masses $m/13$, $m/13^2$, $m/13^3$, etc. and hence linear resolution improved by factors 2.4, 5.5, 13, etc.

As in Nested Splitting, better smoothing is obtained if the desired number of neighbours is evaluated according to equation (18).

In the context of star formation, gravitational collapse and fragmentation are crucial physical processes, and therefore the code must always be able to resolve the Jeans mass. This is called the Jeans Condition (Truelove et al. 1997; Bate & Burkert 1977). As the Jeans mass is a local function of state, it is straightforward to formulate the Jeans Condition, and to split particles when they are about to violate it. We explore On-The-Fly Particle Splitting triggered by the Jeans Condition, in the next two sections.

7 THE JEANS CONDITION

Truelove et al. (1997) have shown that simulations of protostellar collapse and fragmentation performed using AMR only converge when the local Jeans length $\lambda_{\text{Jeans}} \sim a(G\rho)^{-1/2}$ is resolved (where a is the local sound speed). Specifically the linear resolution Δr must everywhere satisfy

$$\Delta r \lesssim \frac{\lambda_{\text{Jeans}}}{4}. \tag{19}$$

Otherwise artificial fragmentation can occur and/or real fragmentation can be suppressed. Equation (19) is the formulation of the Jeans Condition appropriate for FD codes.

Bate & Burkert (1997) have shown that there is a similar Jeans Condition for SPH simulations: the minimum resolvable mass $\sim 2\mathcal{N}_{\text{neib}} m$ must everywhere be less than the local Jeans mass $\sim G^{-3/2}\rho^{-1/2}a^3$, or

$$\frac{G^3 \rho_i m_i^2}{a_i^6} < \frac{1}{(2\mathcal{N}_{\text{neib}})^2} \sim 10^{-4}. \tag{20}$$

Otherwise artificial fragmentation may occur, and real fragmentation will definitely be suppressed.

Whitworth (1998) has shown that provided the smoothing kernel is sufficiently centrally peaked, SPH simulations of collapse are unlikely to suffer from artificial fragmentation. However, it remains the case that equation (20) must be satisfied if real fragmentation is to be modelled.

8 ROTATING COLLAPSE TEST

A standard test of star formation codes is the one proposed by Boss & Bodenheimer (1979; hereafter BB79). In this test the initial conditions are a uniform-density isothermal cloud having mass $M_\odot$, radius 0.02 pc, density 2×10^{-18} g cm^{-3} and isothermal sound speed 0.17 km s^{-1} (so the ratio of thermal to gravitational energy is ~ 0.26). The cloud then has an $m = 2$ azimuthal density perturbation with 10 per cent amplitude imposed on it, and it is set to rotate at uniform angular speed 7.2×10^{-13} rad s^{-1} (so the ratio of rotational to gravitational energy is ~ 0.16). There is no external pressure, and the gas remains isothermal during the subsequent evolution, until the density rises above a critical value $\rho_{\rm crit}$, when it switches to being adiabatic and therefore heats up.

Klein et al. (1999) have performed this test, with $\rho_{\rm crit} = 5 \times 10^{-14}$ g cm^{-3}, using AMR, and shown that the cloud should collapse to produce an elongated structure. This structure then evolves into a binary system with a bar between the components. As long as the gas remains isothermal, the binary components and the interconnecting bar condense into filamentary singularities and the bar does not fragment (Truelove et al. 1998). These results agree with the theoretical analysis of Inutsuka & Miyama (1992), but contrast with earlier simulations of the BB79 test using both FD and SPH codes. In particular, the simulations reported by Burkert & Bodenheimer (1993) resulted in the bar fragmenting. The reason for this appears to have been that their simulations did not satisfy the Jeans Condition.

Bate & Burkert (1997) have subsequently repeated the BB79 test with $\rho_{\rm crit} = 10^{-14}$ g cm^{-3}, using SPH and 80 000 particles, sufficient to satisfy the Jeans Condition up to a density $\sim \rho_{\rm crit}$. They now find essentially the same result as Truelove et al. (1998) and Klein et al. (1999), confirming that the earlier results of Burkert & Bodenheimer (1993) were compromised by violating the Jeans condition. Thus the BB79 test appears to be a stringent test of whether a code is satisfying the Jeans Condition.

We have performed three SPH simulations of the BB79 test. We have required the gas to remain isothermal up to a density $\rho_{\rm crit} = 5 \times 10^{-12}$ g cm^{-3}. This is two orders of magnitude higher than the value used by Klein et al. (1999), and so in our simulations the Jeans mass and length fall to values 10 times smaller, i.e. $M_{\rm Jeans} \sim 10^{-4}\,M_\odot$ and $R_{\rm Jeans} \sim 2$ au. Thus we are subjecting our code to an even sterner test than that advocated by Klein et al. (1999). If one accepts the notion of opacity-limited fragmentation, then in nature the Jeans mass should not fall below $\sim 10^{-3}\,M_\odot$. Therefore – in this limited sense – we are also subjecting our code to a sterner test than that set by nature.

In the standard simulation there are 600 000 particles from the outset, sufficient to satisfy the Jeans condition without Particle Splitting. In the other two simulations there are only 45 000 particles at the outset, and the Jeans condition is accommodated by implementing particle splitting, first Nested Particle Splitting and then On-The-Fly Particle Splitting. The Nested Particle Splitting simulation ends up with $\sim 320\,000$ particles, and the On-The-Fly Particle Splitting simulation ends up with $\sim 140\,000$ particles.

We follow the suggestion of Truelove et al. (1997, 1998) that numerical results should be compared, not at precisely the same elapsed time, but instead when the peak density in the computational domain, $\rho_{\rm peak}$, reaches the same value. In particular we present results when $\rho_{\rm peak} \simeq \rho_{\rm crit} = 5 \times 10^{-12}$ g cm^{-3}, and when $\rho_{\rm peak} \simeq 2 \times 10^{-9}$ g cm^{-3}. The reason for this is that the evolution of a simulation appears to progress slightly more rapidly if the resolution is higher. The same effect was reported by Truelove et al. (1997, 1998) for their AMR simulations.

The plots are all grey-scale column-density images through the central 0.004 pc × 0.004 pc (800 au by 800 au) of the computational domain, viewed down the rotation axis. The calibration of the grey-scale is given in the figure captions. Times are given in terms of the initial freefall time $t_{\rm FF} \simeq 0.03$ Myr.

8.1 Standard high-resolution SPH simulation (no Particle Splitting)

In Fig. 1 we show the results of a simulation of the BB79 test with $\rho_{\rm crit} = 5 \times 10^{-12}$ g cm^{-3}, performed using our standard SPH code with 600 000 constant-mass particles. This simulation has sufficient particles to satisfy the Jeans condition throughout the simulation without Particle Splitting. We note that our SPH code has been developed entirely independently of that used by Bate & Burkert (1997) and differs from that code in several major regards, in particular the integration scheme and the gravity solver.

Fig. 1(a) shows a grey-scale column-density image of the centre of the computational domain at the moment the density in the binary components $\rho_{\rm peak}$ passes $\rho_{\rm crit}$, i.e. at $t = 1.237 t_{\rm FF}$. Both the binary components and the bar connecting them approximate to filamentary singularities, and there is no sign of bar fragmentation.

Fig. 1(b) shows the same region at the end of the simulation, $t = 1.245 t_{\rm FF}$. By this stage the gas in the densest parts, i.e. the binary components, has become adiabatic and heated up. As a result the binary components are approximately circular in projection. However, the interconnecting bar is still isothermal; it continues to approximate to a filamentary singularity and shows no sign of fragmenting.

We re-iterate that this simulation extends the isothermal evolution to $\rho_{\rm crit} = 5 \times 10^{-12}$ g cm^{-3}, which is two orders of magnitude higher than the critical density used by Klein et al. (1999). Therefore it constitutes a very stern test of the validity of the code.

8.2 SPH simulation with Nested Particle Splitting

Fig. 2 shows the result of a simulation of the BB79 test, again with $\rho_{\rm crit} = 5 \times 10^{-12}$ g cm^{-3}, but now performed with only 45 000 equal-mass particles at the outset. Nested Particle Splitting is applied after $t_{\rm split} = 1.244 t_{\rm FF}$, within a cylindrical subdomain of radius 0.003 pc (600 au) and height 0.003 pc (600 au). The symmetry axis of the cylinder is aligned with the rotation axis of the cloud. Its size is chosen so as to contain all regions that become so dense that without Particle Splitting they would eventually violate the Jeans Condition, i.e. the final binary components, which have an orbit of radius 0.002 pc (400 au).

Figs 2(a) and (b) correspond to times $t = 1.258 t_{\rm FF}$ (when $\rho_{\rm peak} \simeq \rho_{\rm crit}$) and $t = 1.265 t_{\rm FF}$ (the end of the simulation at $\rho_{\rm peak} \simeq 2 \times 10^{-9}$ g cm^{-3}). By comparing Figs 1 and 2, we see that the simulation with Nested Particle Splitting reproduces the crucial features of the evolution found in the standard high-resolution simulation described in Section 8.1. As before, a binary system forms with a bar between the components, and as long as the gas remains isothermal the binary components and the bar evolve towards filamentary singularities, with no tendency for additional fragments to condense out of the bar. There is a small density peak at the centre of the bar in the first frame (2a; $\rho_{\rm peak} \simeq \rho_{\rm crit}$), but this quickly disperses, and therefore we do not consider it to be critical.

By the end, approximately half the particles have been split, so there are ∼320 000 particles in total. The simulation with Nested Particle Splitting therefore requires less than half the memory and approximately 25 per cent of the CPU used by the standard simulation (with 600 000 particles, Section 8.1).

8.3 SPH simulation with On-The-Fly Particle Splitting

Finally Fig. 3 shows the result of a simulation of the BB79 test, again with $\rho_{\rm crit} = 5 \times 10^{-12}\,{\rm g\,cm^{-3}}$, and again performed using only 45 000 equal-mass particles at the outset, but now with Particle Splitting applied On-The-Fly, in response to imminent violation of the Jeans Condition.

Figs 3(a) and (b) correspond to times $t = 1.259 t_{\rm FF}$ (when $\rho_{\rm peak} \simeq \rho_{\rm crit}$) and $t = 1.270 t_{\rm FF}$ (the end of the simulation at $\rho_{\rm peak} = 3 \times 10^{-9}\,{\rm g\,cm^{-3}}$; a slightly higher final density than in the other two simulations, see below). Again the simulation reproduces all the critical features reported by Truelove et al. (1998) and Klein et al. (1999), in particular no tendency for additional fragments to condense out of the bar. Once more there is a small density peak at the centre of the bar in the first frame (3a; $\rho_{\rm peak} \simeq \rho_{\rm crit}$), which then quickly disperses.

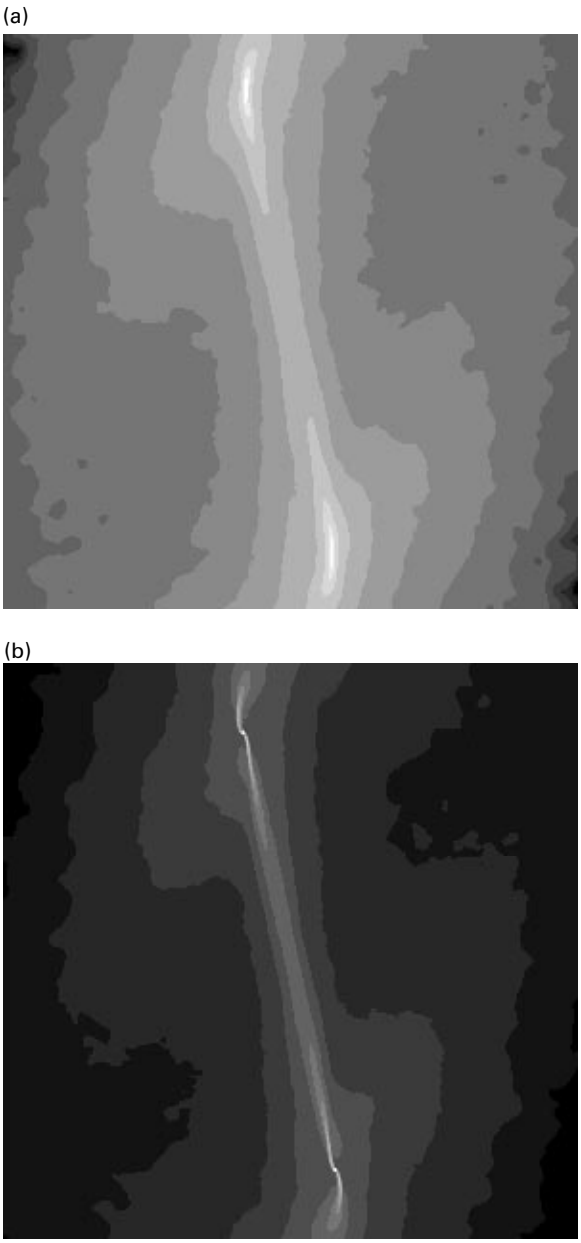

Figure 1. The BB79 test performed using standard SPH with 600 000 constant-mass particles and anticlockwise rotation: column-density images of the central $0.004 \times 0.004\,{\rm pc}^2$ of the computational domain, looking down the rotation axis. (a) At time $t = 1.237 t_{\rm FF}$, when $\rho_{\rm peak} \simeq \rho_{\rm crit} = 5 \times 10^{-12}\,{\rm g\,cm^{-3}}$; the grey-scale is logarithmic, with 16 equal intervals from $3.60 \times 10^{23}\,{\rm H_2\,cm^{-2}}$ to $4.56 \times 10^{25}\,{\rm H_2\,cm^{-2}}$ (or equivalently, adopting solar composition, $1.44\,{\rm g\,cm^{-2}}$ to $1.82 \times 10^{2}\,{\rm g\,cm^{-2}}$). (b) At time $t = 1.245 t_{\rm FF}$ when $\rho_{\rm peak} \simeq 2 \times 10^{-9}\,{\rm g\,cm^{-3}}$; the grey-scale is logarithmic, with 16 equal intervals from $3.72 \times 10^{23}\,{\rm H_2\,cm^{-2}}$ to $1.55 \times 10^{27}\,{\rm H_2\,cm^{-2}}$ (or equivalently $1.49\,{\rm g\,cm^{-2}}$ to $6.19 \times 10^{3}\,{\rm g\,cm^{-2}}$).

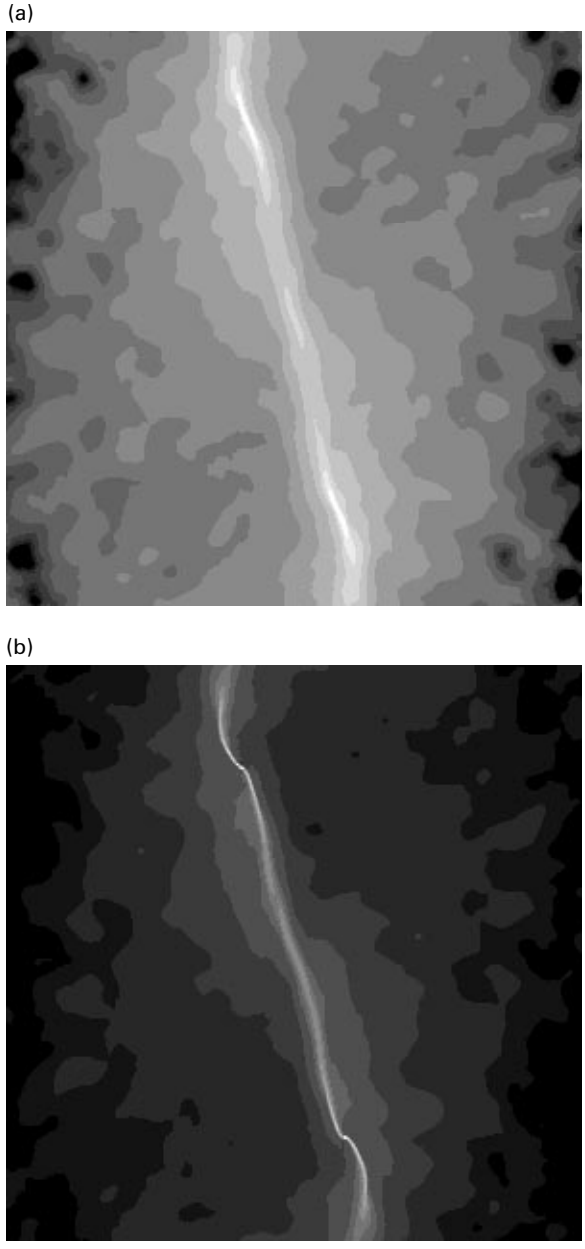

Figure 2. As Fig. 1, but performed using only 45 000 particles initially and then Nested Particle Splitting in a central cylindrical subdomain of radius 0.003 pc and height 0.003 pc. (a) At time $t = 1.258 t_{\rm FF}$, when $\rho_{\rm peak} \simeq \rho_{\rm crit} = 5 \times 10^{-12}\,{\rm g\,cm^{-3}}$. (b) At time $t = 1.265 t_{\rm FF}$ when $\rho_{\rm peak} \simeq 2 \times 10^{-9}\,{\rm g\,cm^{-3}}$.

The only significant difference is a fanning-out of the bar close to the binary components, right at the end of the simulation. This is a real effect, owing to the tidal shearing of the bar by the in-spiraling binary components. It only appears in this simulation because the evolution has been followed to somewhat higher density ($3 \times 10^{-9}\,\mathrm{g\,cm^{-3}}$ instead of $2 \times 10^{-9}\,\mathrm{g\,cm^{-3}}$); hence the binary components have become further out of alignment with the bar, where they can exert a disruptive shear on the ends of the bar.

At the end, less than one fifth of the original particles have been split, so there are $\sim 140\,000$ particles in total. The simulation with On-The-Fly Splitting therefore requires less than one quarter of the memory and less than 10 per cent of the CPU used by the standard simulation (with 600 000 particles, Section 8.1).

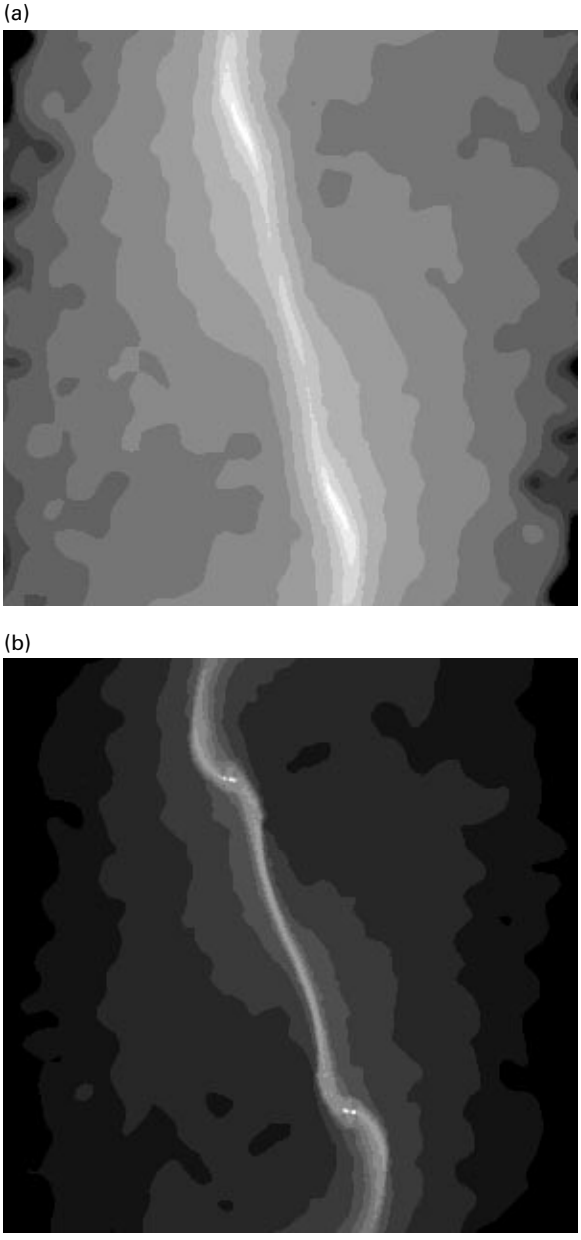

Figure 3. As Fig. 1, but performed using only 45 000 particles initially and then On-The-Fly Splitting triggered above $\rho = \rho_{\mathrm{split}} = 3 \times 10^{-14}\,\mathrm{g\,cm^{-3}}$. (a) At time $t = 1.259 t_{\mathrm{FF}}$, when $\rho_{\mathrm{peak}} \simeq \rho_{\mathrm{crit}} = 5 \times 10^{-12}\,\mathrm{g\,cm^{-3}}$. (b) At time $t = 1.270 t_{\mathrm{FF}}$ when $\rho_{\mathrm{peak}} \simeq 3 \times 10^{-9}\,\mathrm{g\,cm^{-3}}$.

9 DISCUSSION

It appears that Particle Splitting is a viable option for increasing the resolution, locally, during an SPH simulation of self-gravitating collapse. In this context, the most stringent and apposite test of the algorithm is the BB79 test, where extra resolution is required to avoid violating the Jeans Condition (and hence to avoid artificial fragmentation). Acceptable results are obtained for the BB79 test, even when the gas is programmed to stay isothermal up to $\rho_{\mathrm{crit}} = 5 \times 10^{-12}\,\mathrm{g\,cm^{-3}}$. Perturbations arising from the splitting process are transient, and are effectively and quickly damped. Moreover, the simulation is accomplished with much less memory and CPU than a standard simulation, particularly with the On-The-Fly implementation. We note also that the savings in memory and CPU are likely to be far greater in realistic simulations of star formation, where only a fraction of the matter in a cloud collapses to form stars, and therefore a far smaller fraction of particles needs to be split and to be followed with a small time-step.

Other tests have been performed using the two Particle Splitting algorithms. In particular we note the following. (i) We have evolved a static, stable isothermal sphere, contained by an external pressure P_{ext}, and shown (a) that it remains stable, and (b) that its density profile is not corrupted. The configuration treated has mass $\mathrm{M}_{\odot}$, radius 0.01 pc, and temperature 7.9 K. It is quite centrally condensed, with $\rho_{\mathrm{central}} \simeq 3\rho_{\mathrm{edge}}$ and $P_{\mathrm{ext}} \simeq 3 \times 10^{-12}\,\mathrm{erg\,cm^{-3}}$. (ii) We have also followed the collapse of an isothermal cloud which initially has uniform density, and quickly evolves towards an inverse-square density profile ($\rho \propto r^{-2}$). The cloud has mass $\mathrm{M}_{\odot}$ and temperature 7.9 K. Initially it has radius 0.016 pc and uniform density $\sim 4 \times 10^{-18}\,\mathrm{g\,cm^{-3}}$. The effect of Particle Splitting on the ensuing collapse is negligible.

Particle Splitting might be applied in other situations where increased resolution is required locally. The Nested implementation requires prior knowledge of where extra resolution will be required. The On-The-Fly implementation requires that the condition for requiring extra resolution can be formulated as a local function of state. However, more development and testing is needed to establish the stability of the method in these more general situations.

One difference between Particle Splitting and AMR is that Particle Splitting – at least in its present form – is irreversible. If fluid flows into, and then out of, a region where extra resolution is required, particles become split and stay split. However, there is no a priori reason why particles should not be merged in regions where they are delivering much higher resolution than is required by the local physics, and indeed this was done successfully by both Monaghan & Varnas (1988) and Meglicki et al. (1993), using a grid. We have not yet attempted to do this, so we cannot comment further on its feasibility.

The concern is that, without merging, if a single low-mass particle is surrounded by high-mass particles, equation (18) dictates that it has very few neighbours (typically only four if the surrounding particles are 13 times more massive). Therefore the low-mass particle might have rather noisy density, pressure, etc. because of small-number statistics and sudden changes in its neighbour list. However, this will be to a large extent offset by two factors. First, by implication the fluid is well resolved by the large particles, so they have a well relaxed distribution and the neighbourhood of the low-mass particle should be quite constant. Secondly, as regards the macroscopic continuum properties of the fluid, within the sphere of influence of the low-mass particle (i.e. within its smoothing kernel) it makes only a ~ 2 per cent

contribution to the local thermodynamic variables, and so fluctuations in its individual properties are very diluted.

Shocks and ionization fronts can be treated effectively using ellipsoidal kernels (Owen et al. 1998; Francis 2001). Moreover, in the context of star formation, irreversibility may not be a serious problem, because once gravitational collapse and fragmentation are underway the local Jeans mass is unlikely to increase much, and so the resolution required by the Jeans Condition is unlikely to decrease. We are currently developing a version of our code which treats magnetic fields and ambipolar diffusion (Hosking & Whitworth, in preparation), but until this has been fully tested without particle splitting it would not be sensible to combine the two.

10 CONCLUSIONS

We have described how Particle Splitting can be implemented in SPH, and we have shown that it offers a stable and economic way to increase the local resolution of an SPH simulation of self-gravitating collapse, and hence avoid violating the Jeans Condition. This makes Particle Splitting a useful refinement for SPH simulations of gravitational collapse and fragmentation.

ACKNOWLEDGMENTS

The authors thank Henri Boffin and Neil Francis for many interesting discussions on this project.

REFERENCES

Barnes J., Hut P., 1986, Nat, 324, 446
Bate M. R., Burkert A., 1997, MNRAS, 288, 1060
Bate M. R., Bonnell I. A., Price N. M., 1995, MNRAS, 277, 362
Berger M. J., Colella P., 1989, J. Comp. Phys., 82, 64
Boss A. P., Bodenheimer P., 1979, ApJ, 234, 289 (BB79)
Burkert A., Bodenheimer P., 1993, MNRAS, 264, 798
Francis N., 2001, PhD thesis (Cardiff University)
Gingold R. A., Monaghan J. J., 1977, MNRAS, 181, 375
Hernquist L., 1987, ApJS, 64, 715
Hernquist L., Katz N., 1989, ApJS, 70, 419
Inutsuka S., Imaeda Y., 2001, Computational Fluid Dynamics Journal, 9, 316
Inutsuka S., Miyama S. M., 1992, ApJ, 388, 392
Kessel-Deynet O., Burkert A., 2000, MNRAS, 315, 713
Klein R. I., Fisher R. T., McKee C. F., Truelove J. K., 1999, in Miyama S. M., Tomisaka K., Hanawa T., eds, Astrophysics & Space Science Library, Vol. 240, Numerical Astrophysics 1998. Kluwer Academic, Boston, p. 131
Lattanzio J. C., Monaghan J. J., Pongracic H., Schwarz M. P., 1985, MNRAS, 215, 125
Lucy L. B., 1977, AJ, 82, 1013
Meglicki Z., Wickramasinghe D., Bicknell G. V., 1993, MNRAS, 264, 691
Monaghan J. J., 1992, ARA&A, 30, 543
Morris J. P., Monaghan J. J., 1997, J. Comp. Phys, 136, 41
Monaghan J. J., Lattanzio J. C., 1985, A&A, 149, 135
Monaghan J. J., Varnas S. R., 1988, MNRAS, 231, 515
Nelson R. P., Langer W. D., 1997, ApJ, 482, 796
Nelson R. P., Papaloizou J. C. B., 1993, MNRAS, 265, 905
Nelson R. P., Papaloizou J. C. B., 1994, MNRAS, 270, 1
Owen J. M., Villumsen J. V., Shapiro P. R., Martel H., 1998, ApJS, 115, 155
Salmon J. K., Warren M. S., Winckelmans G. S., 1994, Int J. Supercomputer Applications and High Performance Computing, 8, 129
Truelove K. J., Klein R. I., McKee C. F., Holliman J. H., Howell L. H., Greenhough J. A., 1997, ApJ, 489, L179
Truelove K. J., Klein R. I., McKee C. F., Holliman J. H., Howell L. H., Greenhough J. A., Woods D. T., 1998, ApJ, 495, 821
Turner J. A., Chapman S. J., Bhattal A. S., Disney M. J., Pongracic H., Whitworth A. P., 1995, MNRAS, 277, 705
Watkins S. J., Bhattal A. S., Francis N., Whitworth A. P., 1995, A&AS, 119, 177
Whitworth A. P., 1998, MNRAS, 296, 442

This paper has been typeset from a TEX/LATEX file prepared by the author.